Editors' Suggestion

Dimming Starlight with Dark Compact Objects

Joseph Bramante,[1,2,3,*] Melissa D. Diamond,[1,2,3,†] and J. Leo Kim[1,2,‡]
[1]Department of Physics, Engineering Physics, and Astronomy, Queen's University, Kingston, Ontario K7L 3N6, Canada
[2]Arthur B. McDonald Canadian Astroparticle Physics Research Institute, Kingston, Ontario K7L 3N6, Canada
[3]Perimeter Institute for Theoretical Physics, Waterloo, Ontario N2J 2W9, Canada

(Received 16 October 2024; accepted 20 February 2025; published 8 April 2025)

We demonstrate a new technique to search for dark compact objects. When dark matter comprising a dark compact object interacts with photons, the compact object can disperse light traveling though it. As these objects pass between Earth and a distant star, they act as "lampshades" that dim the star. We examine how dimming effects from clumps of dark matter in the Galaxy could be searched for in microlensing surveys, which measure the brightness of stars as a function of time. Using the EROS-2 and OGLE surveys, we show that a dimming analysis of existing data can be used to constrain dark sectors and could be used to discover dark matter in compact objects.

DOI: 10.1103/PhysRevLett.134.141001

Introduction—Primordial black holes (PBHs) [1,2] and massive compact halo objects (MACHOs) are of great interest for beyond-standard model (BSM) studies of the Universe, both as dark matter (DM) candidates (see, e.g., Refs. [3–5]) and as natural consequences of many self-interacting dark sectors and exotic cosmologies [6–25]. There are several ways to observe and constrain these objects [26–39]. Prominent among them are microlensing [40] searches, which look for the amplification of starlight from a bright source due to gravitational lensing from an intermediate heavy object. Microlensing surveys, such as EROS-2 [41], OGLE [42,43], and Subaru Hyper Suprime-Cam (HSC) [44], have played an essential role in the hunt for BSM physics—providing some of the most sensitive probes of PBHs and MACHOs in the $10^{-10}M_\odot$–$10M_\odot$ mass range [45].

While microlensing searches traditionally focus on extremely compact and heavy objects, recent works [46,47] (and sources contained in Ref. [48]) have demonstrated that microlensing constraints change significantly for extended DM lenses. Further, these surveys may be sensitive to objects too light or diffuse to act as traditional lenses. Dark compact objects with weak interactions with the standard model (SM) can scatter starlight. When they pass between Earth and a distant source star this scattering dims the incoming starlight like a lampshade. Microlensing surveys, which are sensitive to slight changes in the brightness of distant stars as a function of time, are well equipped to look for this dimming. Excitingly, these dimming effects are most observable for objects microlensing surveys are otherwise insensitive to, broadening their reach.

In this Letter, we study how diffuse, self-gravitating clouds of DM which interact with SM photons dim starlight. The idea is similar to Ref. [49], which studied how dark exoplanets gravitationally bound to a source star can dim the source starlight and be observed in exoplanet searches. Here we consider free-floating dark structures in the Galaxy, which can enter the observing tube between the source star and the local observer. In particular, we adapt the existing microlensing events formalism [50,51] for dimming events by defining a dimming event as a drop in apparent magnitude and by replacing the Einstein radius of the object with its physical radius.

We show various microlensing surveys' sensitivities to dimming effects, which are summarized in Fig. 1. As the amount of dimming depends on the SM photon-DM interaction, we first show how dimming effects could constrain a general mass and photon scattering cross section of the DM particles that make up the compact structures. We then show how dimming effects could be used to place complementary constraints on a specific DM model, using millicharged DM [52] as an example. We show that null observations of dimming events may place competitive bounds on millicharged particles confined in compact objects. We remain agnostic about how these dark compact objects form, but note that many mechanisms for MACHO formation in the early Universe have been identified recently [6–25].

Dimming from dark matter lampshades—To determine stellar dimming by DM objects, we treat the source star as pointlike and consider an extended spherical DM cloud with constant density ρ_χ, unless otherwise specified, and

*Contact author: joseph.bramante@queensu.ca
†Contact author: m.diamond@queensu.ca
‡Contact author: leo.kim@queensu.ca

Published by the American Physical Society under the terms of the Creative Commons Attribution 4.0 International license. Further distribution of this work must maintain attribution to the author(s) and the published article's title, journal citation, and DOI. Funded by SCOAP³.

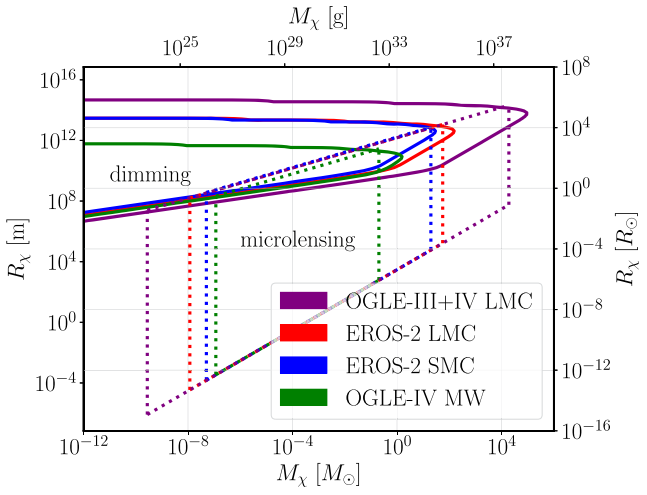


FIG. 1. Heuristic plot showing various microlensing surveys' sensitivity to DM clumps assuming that $R_{\chi,\mathrm{eff}} \approx R_\chi$. Surveys are sensitive to dimming in the region enclosed by the solid curves, whereas surveys are sensitive to microlensing inside the dashed lines [46].

physical radius R_χ. The transmittance (i.e., the amount of starlight that passes through the DM cloud) at a position a distance r from the center of the cloud is given by

$$T(r) = \exp\left(-2\tau_0\sqrt{1-(r/R_\chi)^2}\right), \tag{1}$$

where $\tau_0 \equiv R_\chi n_\chi \sigma$ is the characteristic optical depth of the DM cloud. The cross section σ describes the interactions between DM particles and photons that cause dimming, and $n_\chi = \rho_\chi/m_\chi$ is the number density of the χ particles in the DM cloud. To trigger a dimming event, we require a minimum fraction μ_0 of light be blocked by the cloud. This occurs at an effective radius

$$R_{\chi,\mathrm{eff}} = R_\chi\sqrt{1-\frac{1}{4\tau_0^2}[\ln(1-\mu_0)]^2}. \tag{2}$$

The multiplicative factor on the right-hand side of Eq. (2) is analogous to the usual impact parameter u_T in the case of microlensing [50]. Here, we consider the dimming from a compact object transit to be detectable if the background source passes within $R_{\chi,\mathrm{eff}}$ of the center of the DM sphere. Note that Eq. (2) gives a minimum value of τ_0 to get a real solution, which is given by $\tau_{0,\mathrm{min}} = \frac{1}{2}\ln(1-\mu_0)$. Therefore, if a dimming event occurs, the measured flux of the source star is diluted to a fraction $1-\mu_0 = 10^{(\bar{m}-m_{\mathrm{dim}})/2.5}$, where m_{dim} is the dimmed apparent magnitude and $\bar{m}$ is the fiducial apparent magnitude of the source.

For a given value of the characteristic optical depth τ_0, the size of the DM cloud can be determined by the dip in magnitude. Microlensing surveys set a minimum total amplification to register a lensing event, given conventionally by $\mu_T = 1.34$ [40]—i.e., a 34% amplification. No convention exists for dimming, so we choose $\mu_0 = 0.34$ as the fiducial value throughout this Letter so that a dimming event occurs when 34% of the starlight is dimmed. If a fiducial value of $\mu_0 = 0.34$ is selected, then $R_{\chi,\mathrm{eff}} \approx R_\chi$ for $\tau_0 \geq 1$. Hereafter, we work with $\tau_0 = 1$ unless stated otherwise.

Especially for lower dimming thresholds (i.e., 1%), it will be important to consider other astrophysical sources of star dimming, e.g., exoplanets, which are an active topic of research. Assuming 0.1 Jupiter-size exoplanets per star equally distributed from 1–100 A.U. [53], we estimate $\mathcal{O}(100)$ 1% dimming events in an OGLE-like 20 yr dataset (removing planets that would be identifiable by orbiting repeatedly during the survey time). To differentiate between background dimming events and those from DM clumps, a careful light curve analysis could be employed, which is beyond the scope of this Letter. Prior work in Ref. [49] has shown that mock light curves from dark exoplanets and regular exoplanets are differentiable so long as the transiting object is sufficiently large and translucent. In the future, it may be fruitful to conduct a similar study for microlensing-style surveys.

Dimming event rates—We model the dimming event rates by modifying the procedure used for microlensing [46,47]. We assume all DM clumps have a mass M_χ and velocities set by a Maxwell-Boltzmann distribution. We assume that the line-of-sight density of clumps in the Galaxy is given by $\rho_{\mathrm{clumps}}(x) = f_{\mathrm{DM}}\rho_{\mathrm{DM}}(x)$, where f_{DM} is the fraction of DM residing in these clumps and ρ_{DM} is the position-dependent DM density. Note that we have used the conventional variable $x = D_L/D_S$ to parametrize distances, where D_L is the distance to the clump (normally the gravitational lens in microlensing scenarios), and D_S is the distance to the source field. The DM density for the Milky Way (MW) is modeled assuming an isothermal profile

$$\rho_{\mathrm{DM}}[r(x)] = \frac{\rho_s}{1+[r(x)/r_s]^2}, \tag{3}$$

where $r_s = 4.38$ kpc is the central scale radius, and

$$r(x) = \sqrt{R_{\mathrm{Sol}}^2 - 2xR_{\mathrm{Sol}}D_S\cos\ell\cos b + x^2D_S^2}, \tag{4}$$

in which $R_{\mathrm{Sol}} = 8.5$ kpc is the distance to the Sun and $\rho_s = 1.39\ \mathrm{GeV/cm^3}$ is the central density [54]. The differential event rate for microlensing events is given by [50,51]

$$\frac{d^2\Gamma}{dxdt_E} = \varepsilon(t_E)\frac{2D_S}{v_0^2M_\chi}f_{\mathrm{DM}}\rho_{\mathrm{DM}}(x)v_E^4(x)e^{-v_E^2(x)/v_0^2}, \tag{5}$$

where $v_0 = 220$ km/s is the circular speed of DM in our Galaxy, v_E is the relative velocity of the lensing system for the duration of the event, and $\varepsilon(t_E)$ is the so-called efficiency parameter. We take a constant value of $\varepsilon(t_E) = 1$, as evaluating the efficiency parameter for dimming is outside the scope of this Letter. Given this rate, the resulting

number of events is

$$N_{\text{events}} = N_* T_{\text{obs}} \int_0^1 dx \int_{t_{E,\min}}^{t_{E,\max}} dt_E \frac{d^2\Gamma}{dx dt_E}, \tag{6}$$

where $t_{E,\min}$ ($t_{E,\max}$) is the minimum (maximum) timescale that the survey is sensitive to, N_* is the number of stars in the source field, and T_{obs} is the total observing time of the survey.

Next we note that $t_{E,\min}$ and $t_{E,\max}$ are determined by the behavior of their respective efficiency parameters, which are related to the observing cadence and total observation time of the detector. Here we will use the minimum and maximum event times computed by the microlensing surveys [41,55–57], except for OGLE-III+IV, where we have taken $t_{E,\max} = 7300$ days (corresponding to 20 yr) rather than the 10 000 days the analysis was performed up to. The microlensing event rate and count can easily be recast for dimming effects. The primary difference comes from considering the physical radii of the clumps rather than their Einstein radii [46,47]. In our case, $v_E = 2R_{\chi,\text{eff}}/t_E$.

We consider four source fields in our analysis: the EROS-2 surveys of the Large Magellanic Cloud (LMC) and the Small Magellanic Cloud (SMC) [41], the 5 yr dataset from the OGLE-IV survey of the Milky Way bulge [55], and the 20 yr dataset from the combined OGLE-III [42] and OGLE-IV [43] (henceforth, OGLE-III+IV) surveys of the LMC [56,57]. The survey parameters needed to estimate the event rate are summarized in Table I. We have taken the relevant values for EROS-2 and OGLE-IV from Ref. [46] and adopted parameters from Refs. [56,57] for OGLE-III +IV. For simplicity, we considered the same range of event times for dimming events as previous microlensing studies. Note that, while there is an 8 yr dataset for the OGLE-IV survey of the Milky Way bulge [58], we have used the 5 yr dataset for comparison with Ref. [46] and also since any constraints from the 8 yr dataset will be weaker than the 20 yr OGLE-III+IV dataset of the LMC.

As already mentioned, Fig. 1, which can be compared to microlensing mass reach figures in Refs. [46,47], shows a heuristic estimate of the masses M_χ and physical radii R_χ of spherical DM clumps accessible to EROS-2, OGLE-IV, and OGLE-III+IV microlensing surveys. We do not assume a specific density profile in this figure. To demonstrate the sensitivity of a survey to dimming and microlensing events, all enclosed regions have at least one event following Eq. (6). The regions enclosed by the solid curves are where the surveys are sensitive to dimming effects, while the regions enclosed by dotted lines are where the surveys would be sensitive to microlensing. Note that the region for sensitivity for microlensing presented in Fig. 1 is different from that shown in Ref. [46], since we are considering a detection efficiency of $\varepsilon(t_E) = 1$ for both microlensing and dimming to present a fair comparison between "best-case" scenarios. We have also used full observation event time ranges for microlensing presented in Table I instead of a range where the efficiency parameter was roughly constant, as in Ref. [46].

While microlensing events are generally only observable when the physical radius of the lens is smaller than its Einstein radius, dimming can occur in objects that are much larger and more diffuse. Dimming allows for detection not only of larger clumps than microlensing does, between $10^{-2}R_\odot$ and $10^6 R_\odot$ depending on the survey, but also lower mass clumps, since dimming depends on the density profile instead of the clump mass.

While Fig. 1 implies dimming sensitivity for arbitrarily small clump masses, in practice there will be a lower cutoff in M_χ for the sensitivity region. This will occur when the clump does not have enough material to observably dim starlight, which will depend on the density profile of the object and the chosen interaction with the SM photon. Without specifying an explicit relationship for a density profile between M_χ and R_χ, the number of events N_{events} will continue to increase as M_χ decreases due to there being more clumps, cf. Eq. (5). Note that, in Fig. 1, we assume that the effective dimming radius is equal to the clump radius. $R_{\chi,\text{eff}} \approx R_\chi$, to demonstrate the best-case scenario for sensitivity to dimming effects. As OGLE-III+IV has the largest region of sensitivity, for the remainder of this Letter we focus only on OGLE-III+IV.

For a clump of constant density $M_\chi = 4\pi\rho_\chi R_\chi^3/3$. Its radius is then given by

$$R_\chi = \sqrt{\frac{3}{4\pi}\frac{\sigma M_\chi}{m_\chi \tau_0}}. \tag{7}$$

With a set density profile, N_{events} no longer monotonically decreases as a function of M_χ, and so a minimum mass can

TABLE I. Table of characteristic information of microlensing surveys used for Fig. 1, modified from Ref. [46] which used data from Ref. [59], with additional data pertaining to OGLE-III+IV [56,57].

Survey	Source	(D_S (kpc), ℓ, b)	N_*	T_{obs} (days)	t_E (days)
EROS-2 [41]	LMC	(50, 280.46°, −32.89°)	5.49×10^6	2500	[1, 1000]
	SMC	(60, 302.81°, −44.33°)	0.86×10^6		
OGLE-IV [55]	MW	(8.5, 1.09°, −2.39°)	4.88×10^7	1826	[0.1, 300]
OGLE-III+IV [56,57]	LMC	(50, 280.46°, −32.89°)	7.87×10^7	7300	[1, 7300]

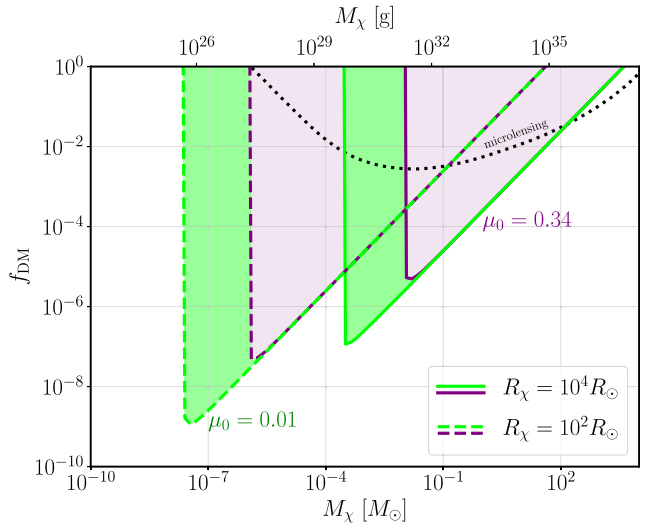


FIG. 2. Limits on the fraction of DM $f_{\rm DM}$ inside clumps of mass M_χ and fixed size $R_\chi = 10^4 R_\odot$ in solid curves and $R_\chi = 10^2 R_\odot$ in dashed curves, assuming null observations of dimming events in OGLE-III+IV. The regions enclosed and shaded in purple assume a dimming of $\mu_0 = 0.34$, while the lime green regions assume a dimming of $\mu_0 = 0.01$. We have fixed $\sigma/m_\chi = 10^2$ GeV^{-3}. The dotted curves in black show restrictions on $f_{\rm DM}$ assuming microlensing from point sources from OGLE-III+IV [56,57].

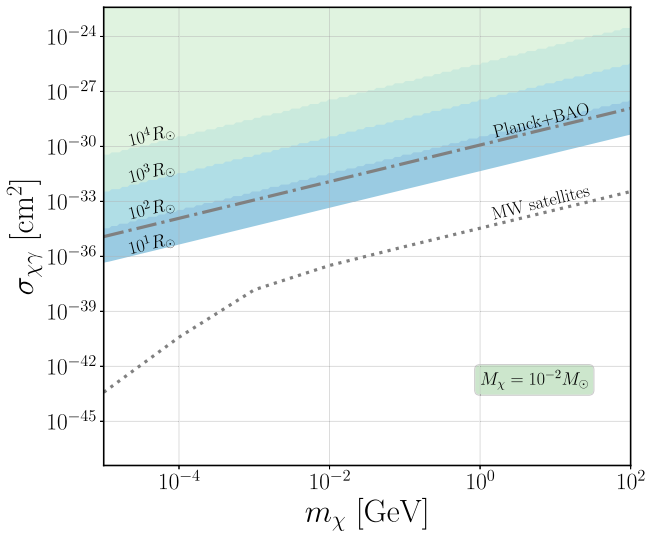


FIG. 3. Possible constraints on m_χ and $\sigma_{\chi\gamma}$ for elastic scattering of SM photons and χ particles from a future null analysis of dimming events in the OGLE-III+IV surveys, assuming fixed physical sizes R_χ between 10 and $10^4 R_\odot$, and a fixed mass of $M_\chi = 10^{-2} M_\odot$. We have assumed that these objects make up $f_{\rm DM} = 0.1$ of the DM. The overlaid gray dash-dotted lines are bounds on the elastic scattering cross section from Planck + BAO [61], while the gray dotted line is bounds from MW satellite galaxies [62]. Note that these constraints are calculated for free-floating DM with $f_{\rm DM} = 1$ and may not be applicable to the scenario shown in this plot.

be obtained. One can fix R_χ and solve for τ_0 using Eq. (7), then compute the effective radius $R_{\chi,\rm eff}$ in Eq. (2) if $\tau_0 > \tau_{0,\rm min}$ so that $R_{\chi,\rm min}$ is real and nonzero. Figure 2 demonstrates how constraints on $f_{\rm DM}$ would look for clumps of fixed physical size. To compute these limits on $f_{\rm DM}$, we have taken $N_{\rm thresh} = 3.9$ events as the threshold number of events required for a 90% confidence level observation of a single event, following Poisson statistics [46]. The regions shaded above the curves indicate $N_{\rm events} \geq N_{\rm thresh}$, where null observations of dimming events in OGLE-III+IV could be used to set constraints for a fraction of DM, $f_{\rm DM}$, at a given DM clump mass. The constraints cut off suddenly for low values of M_χ due to the optical depth's dependence on clump mass, $\tau_0 \propto M_\chi$, given in Eq. (7). When M_χ is large enough, the clumps become opaque and $R_{\chi,\rm eff} \approx R_\chi$. Conversely, decreasing M_χ drives down the implied optical depth τ_0. As is apparent in Eq. (2) the effective radius quickly becomes zero once the required optical depth τ_0 becomes too large. The low mass cutoff occurs for $\tau_0 \approx \tau_{0,\rm min}$, where $M_{\chi,\rm min} = 2\pi m_\chi R_\chi^2 \ln(1-\mu_0)/(3\sigma)$, so the minimum observable mass is determined by the minimum dimming required for an event observation.

Dark matter-photon elastic scattering—While previously we related the number of expected dimming events to the macroscopic properties of the DM clumps, we now show how dimming effects can be used to constrain the microscopic properties of DM comprising the clumps. This is explicitly detailed for elastic DM-SM photon scattering and for millicharged DM. By considering dimming due to elastic scattering $\chi\gamma \to \chi\gamma$ between DM particles and SM photons, Fig. 3 shows how the null observation of dimming events in OGLE-III+IV would constrain m_χ–$\sigma_{\chi\gamma}$ parameter space, assuming various fixed physical radii for clump masses of $M_\chi = 10^{-2} M_\odot$. The high-m_χ, low-$\sigma_{\chi\gamma}$ behavior of the constraints is due to the DM objects becoming too small for detection. Note that, at a fixed clump radius, more massive objects are generally more constrained, which is discussed further in Supplemental Material [60]. However, since $N_{\rm events} \propto M_\chi^{-1}$ in the high clump mass limit, these constraints eventually vanish below $N_{\rm thresh}$.

We have also plotted constraints on $\sigma_{\chi\gamma}$ from analyses of Planck and baryonic acoustic oscillation (BAO) data [61], as well as constraints from considering the population of MW satellites [62]. However, we note that these constraints have assumed that all of DM is able to interact with the SM photon. While they are expected to weaken as one decreases the fraction of DM that is able to interact with the SM photon, their exact behavior under these circumstances remains unknown. The constraints described in Ref. [62] that rely on DM photon scattering that wash out small scale DM structures may behave quite differently than expected in Ref. [62] in the case where all of the χ reside in compact objects. Therefore, when the χ particles responsible for dimming are a subdominant component of DM, dimming effects could provide competitive bounds for $m_\chi > 10^{-3}$ GeV.

Millicharged dark matter—Next we demonstrate how the lampshade effect can be used to search for millicharged DM. Here we assume a simple asymmetric dark sector, containing a dark Dirac fermion χ with mass m_χ and a light dark photon V_μ, which kinetically mixes with the SM photon A_μ,

$$\mathcal{L} \supset \bar{\chi}(i\not{D} - m_\chi)\chi - \frac{1}{4}V_{\mu\nu}V^{\mu\nu} - \frac{\epsilon}{2}V_{\mu\nu}F^{\mu\nu}, \tag{8}$$

where $F_{\mu\nu} = \partial_\mu A_\nu - \partial_\nu A_\mu$ is the usual field strength tensor for the SM photon and $V_{\mu\nu}$ is similarly defined for the dark photon, so the last term in Eq. (8) is a kinetic mixing term with a kinetic mixing parameter ϵ. $D_\mu = \partial_\mu - ig_D V_\mu$ is the covariant derivative with $\alpha_D = g_D^2/(4\pi)$. We assume the dark photon obtains a mass from a Stueckelberg field charged under both the dark and SM Abelian gauge groups, which implies that χ will be electromagnetically millicharged [63,64]. For simplicity, we fix parameters so that χ's have effective SM electric charge $q_\chi = \epsilon g_D/e$, where e is the SM electromagnetic coupling. We note that, for a sufficiently light dark photon, present bounds permit the mixing parameter ϵ to be large, e.g., [65,66]. This class of models [52] has been widely studied both as a BSM particle and a DM candidate (see, e.g., [67–73]).

SM photons passing through a dark clump can undergo various interactions with χ particles. Both scattering, $\chi\gamma \to \chi\gamma$, and conversion to dark photons, $\chi\gamma \to \chi\gamma'$, will cause apparent dimming. The scattering cross section is of order $\mathcal{O}(\epsilon^4)$, while the conversion cross section is of order $\mathcal{O}(\epsilon^2)$, making it the dominant process for dimming in our analysis. In the low energy limit, the $\chi\gamma \to \chi\gamma'$ cross section is given by the Thomson cross section multiplied by a kinetic mixing parameter, $\sigma = 8\pi\alpha_D^2\epsilon^2/(3m_\chi^2)$.

While we have assumed that parameters in the event rate expressions (5) and (6) for dimming events were similar to those of microlensing, different parameters can lead to higher sensitivities (and therefore stronger constraints). In particular, while the minimum event time for microlensing in OGLE-III+IV was $t_{E,\min} = 1$ day [56,57], if the efficiency for dimming effects was permitted to be nonzero at lower event times, then the surveys would be sensitive to smaller sizes. Some microlensing surveys, such as Subaru-HSC [44], and upcoming surveys such as the Legacy Survey of Space and Time (LSST) at the Vera Rubin Observatory [74] and the *Roman* telescope [75], have already considered using much lower event times. Existing analyses also consider reduced minimum event time of 2 min [47] and 15 min [76–78], respectively. Additionally, if the threshold for a minimum amount of dimming was lower rather than $\mu_0 = 0.34$ (chosen to mirror the amplification factor for microlensing), then the surveys could be more sensitive to more dilute DM clumps. A lower threshold for dimming is feasible since OGLE is sensitive to variations in brightness at the millimagnitude level [43].

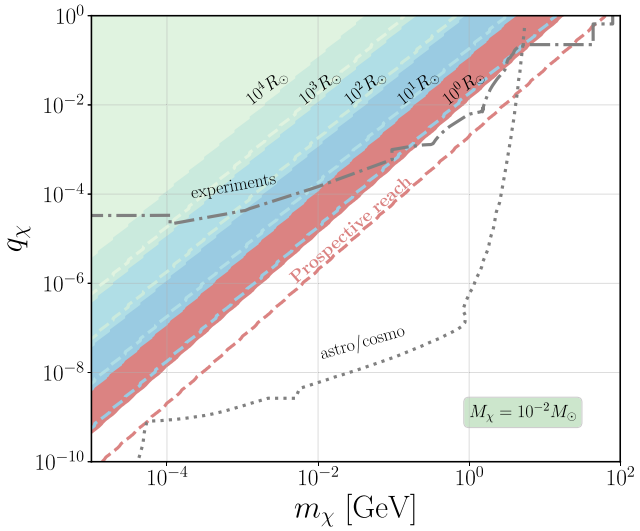


FIG. 4. Similar to Fig. 3, but for the effective fractional charge q_χ for millicharged DM, assuming a minimum event time of $t_{E,\min} = 0.01$ days. The shaded regions assume a dimming fraction of $\mu_0 = 0.34$ while the dashed lines assume a lower dimming of $\mu_0 = 0.01$ for the same color. We have indicated in red the constraints for a prospective reach, where due to the smaller minimum event time we are more sensitive to smaller objects. All other shaded regions remain unchanged in the case with $t_{E,\min} = 1$ day. Only m_χ and q_χ are varied between the curves, with $\alpha_D = 0.1$. Overlaid dotted lines labeled astro-cosmo correspond to a combination of constraints from SN1987A [79,80], stellar evolution [81,82], and limits on $\Delta N_{\rm eff}$ from BBN and CMB [81,83]. Overlaid dotted-dashed lines correspond to constraints from a variety of experiments, including colliders [84], SLAC [85], OPOS [86], ArgoNeuT [87], BEBC [88] and milliQan [89].

To demonstrate these effects, Fig. 4 shows limits on m_χ and q_χ assuming a lower minimum event time of $t_{E,\min} = 0.01$ days for two different dimming thresholds. The shaded areas correspond to a dimming of $\mu_0 = 0.34$, while the dashed lines correspond to $\mu_0 = 0.01$. Considering a shorter minimum event time does not change the reach of the constraints at clump sizes already observable with higher event times. Instead, a shorter minimum event time renders surveys sensitive to smaller clumps which otherwise transit a star too quickly to be seen. Clumps with physical sizes $R_\chi \geq 10R_\odot$ are already detectable at $t_{E,\min} = 1$ day (indicated in blue and green shaded areas), whereas clumps with sizes $R_\chi = R_\odot$ were not detectable at the higher minimum event time.

There are also constraints on millicharged DM in this region of parameter space from interstellar gas cloud cooling [90–94], which will depend nontrivially on the modeling of millicharged clumps heating local portions of gas clouds. Additionally, we have not shown the constraint obtained by requiring that the DM-baryon fluid at recombination is completely decoupled [95], as this is a stronger cosmological condition than necessary.

Conclusion—In this Letter, we have shown how existing microlensing surveys can observe dimming of distant stars due to transits of clouds of DM that interact with photons. We have shown that microlensing surveys are more sensitive to dimming effects than microlensing events for DM clumps (cf. [47]) larger than the Einstein radius of the object. The null observation of dimming effects in microlensing surveys such like EROS-2 and OGLE-III+IV could be used to limit the size, mass, and abundance of DM clumps, as well as limit the microphysical properties of DM comprising the clumps, such as the mass, photon interaction cross sections, and the effective charge of the DM particle in a millicharged DM scenario. Searching existing survey data for dimming events, which will require no modifications to existing or upcoming microlensing data, would make the constraints suggested in this Letter concrete and is an obvious next step. These searches are complementary or competitive with existing DM-photon interaction searches, depending on the survey observing cadence and sensitivity to changes in source brightness. Further, with dedicated modeling of dimming events, any observed dimming could give insight into the properties and abundance of dark clumps and the DM that composes them. We emphasize that the majority of our analysis was performed model independently. This approach could be used to look for or constrain any dark sector model that interacts with photons and forms compact objects.

We note several additional possible extensions to our treatment. First, we have not considered how the lampshade effect and microlensing might overlap. DM clumps with densities in an intersecting region of sensitivity (cf. Fig. 1) can be both a lampshade and a gravitational lens. Here, the competing dimming and brightening effects could result in a lower number of observed microlensing or dimming events. There are, however, additional signatures to look for, as the star may both brighten and dim during different points in the transit if microlensing and dimming effects dominate at different radii. Second, our analysis can be generalized by considering various density profiles for the dark clumps (see Refs. [46,47] for the effects of density profiles in the case of microlensing) and considering other surveys such as Subaru-HSC [44], as well as the future LSST [74] and *Roman* Space Telescope [75]. These surveys allow for source resolution (see, e.g., Refs. [47,76,77,96]), lower minimum observation times, and better sensitivities to changes in brightness—all of which would result in improved bounds. Finally, we note that considering light from an extended source should increase survey dimming event sensitivity.

Acknowledgments—We thank Gonzalo Alonso-Álvarez, Christopher V. Cappiello, Wendy Crumrine, David Curtin, Audrey Fung, Vera Gluscevic, Przemek Mróz, Nirmal Raj, and Han Wu for useful discussions. The authors and this work were supported by the Arthur B. McDonald Canadian Astroparticle Physics Research Institute, the Natural Sciences and Engineering Research Council of Canada (NSERC), and the Canada Foundation for Innovation. Research at Perimeter Institute is supported by the Government of Canada through the Department of Innovation, Science, and Economic Development and by the Province of Ontario. J. L. K. is supported by an NSERC Canada Graduate Scholarship-Doctoral.

[1] S. Hawking, Gravitationally collapsed objects of very low mass, Mon. Not. R. Astron. Soc. **152**, 75 (1971).
[2] B. J. Carr and S. W. Hawking, Black holes in the early Universe, Mon. Not. R. Astron. Soc. **168**, 399 (1974).
[3] B. Carr, F. Kuhnel, and M. Sandstad, Primordial black holes as dark matter, Phys. Rev. D **94**, 083504 (2016).
[4] A. M. Green and B. J. Kavanagh, Primordial black holes as a dark matter candidate, J. Phys. G **48**, 043001 (2021).
[5] P. Villanueva-Domingo, O. Mena, and S. Palomares-Ruiz, A brief review on primordial black holes as dark matter, Front. Astron. Space Sci. **8**, 87 (2021).
[6] C. Kouvaris and N. G. Nielsen, Asymmetric dark matter stars, Phys. Rev. D **92**, 063526 (2015).
[7] J. Eby, C. Kouvaris, N. G. Nielsen, and L. C. R. Wijewardhana, Boson stars from self-interacting dark matter, J. High Energy Phys. 02 (2016) 028.
[8] A. Maselli, P. Pnigouras, N. G. Nielsen, C. Kouvaris, and K. D. Kokkotas, Dark stars: Gravitational and electromagnetic observables, Phys. Rev. D **96**, 023005 (2017).
[9] L. Amendola, J. Rubio, and C. Wetterich, Primordial black holes from fifth forces, Phys. Rev. D **97**, 081302(R) (2018).
[10] M. I. Gresham, H. K. Lou, and K. M. Zurek, Early Universe synthesis of asymmetric dark matter nuggets, Phys. Rev. D **97**, 036003 (2018).
[11] J. H. Chang, D. Egana-Ugrinovic, R. Essig, and C. Kouvaris, Structure formation and exotic compact objects in a dissipative dark sector, J. Cosmol. Astropart. Phys. 03 (2019) 036.
[12] S. Savastano, L. Amendola, J. Rubio, and C. Wetterich, Primordial dark matter halos from fifth forces, Phys. Rev. D **100**, 083518 (2019).
[13] M. M. Flores and A. Kusenko, Primordial black holes from long-range scalar forces and scalar radiative cooling, Phys. Rev. Lett. **126**, 041101 (2021).
[14] G. Domènech and M. Sasaki, Cosmology of strongly interacting fermions in the early universe, J. Cosmol. Astropart. Phys. 06 (2021) 030.
[15] J. Gurian, D. Jeong, M. Ryan, and S. Shandera, Molecular chemistry for dark matter II: Recombination, molecule formation, and halo mass function in atomic dark matter, Astrophys. J. **934**, 121 (2022).
[16] M. Hippert, J. Setford, H. Tan, D. Curtin, J. Noronha-Hostler, and N. Yunes, Mirror neutron stars, Phys. Rev. D **106**, 035025 (2022).
[17] M. M. Flores, A. Kusenko, L. Pearce, and G. White, Fireball baryogenesis from early structure formation due to Yukawa forces, Phys. Rev. D **108**, L091705 (2023).
[18] J. Gurian, M. Ryan, S. Schon, D. Jeong, and S. Shandera, A lower bound on the mass of compact objects from

dissipative dark matter, Astrophys. J. Lett. **939**, L12 (2022); **949**, L44(E) (2023).
[19] G. Domènech, D. Inman, A. Kusenko, and M. Sasaki, Halo formation from Yukawa forces in the very early Universe, Phys. Rev. D **108**, 103543 (2023).
[20] M. M. Flores, Y. Lu, and A. Kusenko, Structure formation after reheating: Supermassive primordial black holes and Fermi ball dark matter, Phys. Rev. D **108**, 123511 (2023).
[21] S. Roy, X. Shen, M. Lisanti, D. Curtin, N. Murray, and P. F. Hopkins, Simulating atomic dark matter in Milky Way analogs, Astrophys. J. Lett. **954**, L40 (2023).
[22] C. Gemmell, S. Roy, X. Shen, D. Curtin, M. Lisanti, N. Murray, and P. F. Hopkins, Dissipative dark substructure: The consequences of atomic dark matter on Milky Way analog subhalos, Astrophys. J. **967**, 21 (2024).
[23] J. Bramante, M. Diamond, and J. L. Kim, The effect of multiple cooling channels on the formation of dark compact objects, J. Cosmol. Astropart. Phys. 02 (2024) 002.
[24] J. Bramante, C. V. Cappiello, M. D. Diamond, J. L. Kim, Q. Liu, and A. C. Vincent, Dissipative dark cosmology: From early matter dominance to delayed compact objects, Phys. Rev. D **110**, 043041 (2024).
[25] S. Roy, X. Shen, J. Barron, M. Lisanti, D. Curtin, N. Murray, and P. F. Hopkins, Aggressively-dissipative dark dwarfs: The effects of atomic dark matter on the inner densities of isolated dwarf galaxies, arXiv:2408.15317.
[26] G. F. Giudice, M. McCullough, and A. Urbano, Hunting for dark particles with gravitational waves, J. Cosmol. Astropart. Phys. 10 (2016) 001.
[27] K. Van Tilburg, A.-M. Taki, and N. Weiner, Halometry from astrometry, J. Cosmol. Astropart. Phys. 07 (2018) 041.
[28] F.-Y. Cyr-Racine, C. R. Keeton, and L. A. Moustakas, Beyond subhalos: Probing the collective effect of the Universe's small-scale structure with gravitational lensing, Phys. Rev. D **100**, 023013 (2019).
[29] J. A. Dror, H. Ramani, T. Trickle, and K. M. Zurek, Pulsar timing probes of primordial black holes and subhalos, Phys. Rev. D **100**, 023003 (2019).
[30] S. Mishra-Sharma, K. Van Tilburg, and N. Weiner, Power of halometry, Phys. Rev. D **102**, 023026 (2020).
[31] Y. Bai, A. J. Long, and S. Lu, Tests of dark MACHOs: Lensing, accretion, and glow, J. Cosmol. Astropart. Phys. 09 (2020) 044.
[32] D. Croon, S. Ipek, and D. McKeen, Gravitational wave constraints on extended dark matter structures, Phys. Rev. D **107**, 063012 (2023).
[33] I.-K. Chen, M. Kongsore, and K. Van Tilburg, Detecting dark compact objects in Gaia DR4: A data analysis pipeline for transient astrometric lensing searches, J. Cosmol. Astropart. Phys. 07 (2023) 037.
[34] I. Armstrong, B. Gurbuz, D. Curtin, and C. D. Matzner, Electromagnetic signatures of mirror stars, Astrophys. J. **965**, 42 (2024).
[35] H. Banks, D. M. Grabowska, and M. McCullough, Gravitational wave backgrounds from colliding exotic compact objects, Phys. Rev. D **108**, 035017 (2023).
[36] N. Raj, Supernovae and superbursts triggered by dark matter clumps, Phys. Rev. D **109**, 123020 (2024).
[37] T. X. Tran, S. R. Geller, B. V. Lehmann, and D. I. Kaiser, Close encounters of the primordial kind: A new observable for primordial black holes as dark matter, Phys. Rev. D **110**, 063533 (2024).
[38] J. B. Dent, B. Dutta, and T. Xu, Multi-messenger probes of asteroid mass primordial black holes: Superradiance spectroscopy, Hawking radiation, and microlensing, Phys. Lett. B **861**, 139254 (2025).
[39] D. E. Kaplan, X. Luo, N. H. Nguyen, S. Rajendran, and E. H. Tanin, Indirect searches for ultraheavy dark matter in the time domain, Phys. Rev. D **111**, 023041 (2025).
[40] B. Paczynski, Gravitational microlensing by the galactic halo, Astrophys. J. **304**, 1 (1986).
[41] P. Tisserand *et al.* (EROS-2 Collaboration), Limits on the Macho content of the galactic halo from the EROS-2 survey of the magellanic clouds, Astron. Astrophys. **469**, 387 (2007).
[42] A. Udalski, The optical gravitational lensing experiment. Real time data analysis systems in the OGLE-III survey, Acta Astron. **53**, 291 (2003).
[43] A. Udalski, M. K. Szymański, and G. Szymański, OGLE-IV: Fourth phase of the optical gravitational lensing experiment, Acta Astron. **65**, 1 (2015).
[44] H. Niikura *et al.*, Microlensing constraints on primordial black holes with Subaru/HSC Andromeda observations, Nat. Astron. **3**, 524 (2019).
[45] B. Carr, K. Kohri, Y. Sendouda, and J. Yokoyama, Constraints on primordial black holes, Rep. Prog. Phys. **84**, 116902 (2021).
[46] D. Croon, D. McKeen, and N. Raj, Gravitational microlensing by dark matter in extended structures, Phys. Rev. D **101**, 083013 (2020).
[47] D. Croon, D. McKeen, N. Raj, and Z. Wang, Subaru-HSC through a different lens: Microlensing by extended dark matter structures, Phys. Rev. D **102**, 083021 (2020).
[48] D. Croon and S. Sevillano Muñoz, Repository for extended dark matter object constraints, Eur. Phys. J. C **85**, 8 (2025).
[49] Y. Bai, S. Lu, and N. Orlofsky, Dark exoplanets, Phys. Rev. D **108**, 103026 (2023).
[50] K. Griest, Galactic microlensing as a method of detecting massive compact halo objects, Astrophys. J. **366**, 412 (1991).
[51] C. Alcock *et al.* (MACHO Collaboration), The MACHO project first year LMC results: The microlensing rate and the nature of the galactic dark halo, Astrophys. J. **461**, 84 (1996).
[52] B. Holdom, Two U(1)'s and Epsilon charge shifts, Phys. Lett. **166B**, 196 (1986).
[53] A. Cumming, R. P. Butler, G. W. Marcy, S. S. Vogt, J. T. Wright, and D. A. Fischer, The Keck Planet search: Detectability and the minimum mass and orbital period distribution of extrasolar planets, Publ. Astron. Soc. Pac. **120**, 531–554 (2008).
[54] M. Cirelli, G. Corcella, A. Hektor, G. Hutsi, M. Kadastik, P. Panci, M. Raidal, F. Sala, and A. Strumia, PPPC 4 DM ID: A poor particle physicist cookbook for dark matter indirect detection, J. Cosmol. Astropart. Phys. 03 (2011) 051; 10 (2012) E01.
[55] H. Niikura, M. Takada, S. Yokoyama, T. Sumi, and S. Masaki, Constraints on Earth-mass primordial black holes from OGLE 5-year microlensing events, Phys. Rev. D **99**, 083503 (2019).
[56] P. Mróz *et al.*, No massive black holes in the Milky Way halo, Nature (London) **632**, 749 (2024).

[57] P. Mróz *et al.*, Microlensing optical depth and event rate toward the large magellanic cloud based on 20 yr of OGLE observations, Astrophys. J. Suppl. Ser. **273**, 4 (2024).
[58] P. Mróz, A. Udalski, J. Skowron, M. K. Szymański, I. Soszyński, Ł. Wyrzykowski, P. Pietrukowicz, S. Kozłowski, R. Poleski, K. Ulaczyk, K. Rybicki, and P. Iwanek, Microlensing optical depth and event rate toward the galactic bulge from 8 yr of OGLE-IV observations, Astrophys. J. Suppl. Ser. **244**, 29 (2019).
[59] M. Wenger *et al.*, The SIMBAD astronomical database, Astron. Astrophys. Suppl. Ser. **143**, 9 (2000).
[60] See Supplemental Material at http://link.aps.org/supplemental/10.1103/PhysRevLett.134.141001 for further information regarding the calculations and assumptions, as well as additional figures.
[61] N. Becker, D. C. Hooper, F. Kahlhoefer, J. Lesgourgues, and N. Schöneberg, Cosmological constraints on multi-interacting dark matter, J. Cosmol. Astropart. Phys. 02 (2021) 019.
[62] W. Crumrine, E. O. Nadler, R. An, and V. Gluscevic, Dark matter coupled to radiation: Limits from the Milky Way satellites, Phys. Rev. D **111**, 023530 (2025).
[63] D. Feldman, Z. Liu, and P. Nath, The Stueckelberg Z-prime extension with kinetic mixing and milli-charged dark matter from the hidden sector, Phys. Rev. D **75**, 115001 (2007).
[64] F. Kahlhoefer and E. Urdshals, On dark atoms, massive dark photons and millicharged sub-components, Phys. Lett. B **807**, 135601 (2020).
[65] S. Navas *et al.* (Particle Data Group), Review of particle physics, Phys. Rev. D **110**, 030001 (2024).
[66] A. Caputo, A. J. Millar, C. A. J. O'Hare, and E. Vitagliano, Dark photon limits: A handbook, Phys. Rev. D **104**, 095029 (2021).
[67] K. J. Kelly and Y.-D. Tsai, Proton fixed-target scintillation experiment to search for millicharged dark matter, Phys. Rev. D **100**, 015043 (2019).
[68] R. Plestid, V. Takhistov, Y.-D. Tsai, T. Bringmann, A. Kusenko, and M. Pospelov, New constraints on millicharged particles from cosmic-ray production, Phys. Rev. D **102**, 115032 (2020).
[69] C. A. Argüelles Delgado, K. J. Kelly, and V. Muñoz Albornoz, Millicharged particles from the heavens: Single- and multiple-scattering signatures, J. High Energy Phys. 11 (2021) 099.
[70] A. Berlin, J. A. Dror, X. Gan, and J. T. Ruderman, Millicharged relics reveal massless dark photons, J. High Energy Phys. 05 (2023) 046.
[71] X. Gan and Y.-D. Tsai, Cosmic millicharge background and reheating probes, arXiv:2308.07951.
[72] H. Wu, E. Hardy, and N. Song, Searching for heavy millicharged particles from the atmosphere, Phys. Rev. D **110**, 115037 (2024).
[73] A. Berlin and D. Hooper, High-energy neutrinos from millicharged dark matter annihilation in the sun, Phys. Rev. D **110**, 075018 (2024).
[74] Z. Ivezić *et al.*, LSST: From science drivers to reference design and anticipated data products, Astrophys. J. **873**, 111 (2019).
[75] D. Spergel *et al.*, Wide-field infrarred survey telescope-astrophysics focused telescope assets WFIRST-AFTA 2015 report, arXiv:1503.03757.
[76] W. DeRocco, E. Frangipane, N. Hamer, S. Profumo, and N. Smyth, Revealing terrestrial-mass primordial black holes with the Nancy Grace Roman Space Telescope, Phys. Rev. D **109**, 023013 (2024).
[77] W. DeRocco, N. Smyth, and V. Takhistov, New light on dark extended lenses with the Roman Space Telescope, Astrophys. J. Lett. **965**, L3 (2024).
[78] J. Fardeen, P. McGill, S. E. Perkins, W. A. Dawson, N. S. Abrams, J. R. Lu, M.-F. Ho, and S. Bird, Astrometric microlensing by primordial black holes with the Roman Space Telescope, Astrophys. J. **965**, 138 (2024).
[79] J. H. Chang, R. Essig, and S. D. McDermott, Supernova 1987A constraints on sub-GeV dark sectors, millicharged particles, the QCD axion, and an axion-like particle, J. High Energy Phys. 09 (2018) 051.
[80] D. F. G. Fiorillo and E. Vitagliano, Self-interacting dark sectors in supernovae can behave as a relativistic fluid, Phys. Rev. Lett. **133**, 251004 (2024).
[81] H. Vogel and J. Redondo, Dark radiation constraints on minicharged particles in models with a hidden photon, J. Cosmol. Astropart. Phys. 02 (2014) 029.
[82] A. Fung, S. Heeba, Q. Liu, V. Muralidharan, K. Schutz, and A. C. Vincent, New bounds on light millicharged particles from the tip of the red-giant branch, Phys. Rev. D **109**, 083011 (2024).
[83] P. Adshead, P. Ralegankar, and J. Shelton, Dark radiation constraints on portal interactions with hidden sectors, J. Cosmol. Astropart. Phys. 09 (2022) 056.
[84] S. Davidson, S. Hannestad, and G. Raffelt, Updated bounds on millicharged particles, J. High Energy Phys. 05 (2000) 003.
[85] A. A. Prinz *et al.*, Search for millicharged particles at SLAC, Phys. Rev. Lett. **81**, 1175 (1998).
[86] A. Badertscher, P. Crivelli, W. Fetscher, U. Gendotti, S. N. Gninenko, V. Postoev, A. Rubbia, V. Samoylenko, and D. Sillou, An improved limit on invisible decays of positronium, Phys. Rev. D **75**, 032004 (2007).
[87] R. Acciarri *et al.* (ArgoNeuT Collaboration), Improved limits on millicharged particles using the ArgoNeuT experiment at Fermilab, Phys. Rev. Lett. **124**, 131801 (2020).
[88] G. Marocco and S. Sarkar, Blast from the past: Constraints on the dark sector from the BEBC WA66 beam dump experiment, SciPost Phys. **10**, 043 (2021).
[89] A. Ball *et al.* (milliQan Collaboration), Sensitivity to millicharged particles in future proton-proton collisions at the LHC with the milliQan detector, Phys. Rev. D **104**, 032002 (2021).
[90] A. Bhoonah, J. Bramante, F. Elahi, and S. Schon, Calorimetric dark matter detection with galactic center gas clouds, Phys. Rev. Lett. **121**, 131101 (2018).
[91] A. Bhoonah, J. Bramante, F. Elahi, and S. Schon, Galactic Center gas clouds and novel bounds on ultralight dark photon, vector portal, strongly interacting, composite, and super-heavy dark matter, Phys. Rev. D **100**, 023001 (2019).
[92] A. Bhoonah, J. Bramante, S. Schon, and N. Song, Detecting composite dark matter with long-range and contact interactions in gas clouds, Phys. Rev. D **103**, 123026 (2021).

[93] D. Wadekar and G. R. Farrar, Gas-rich dwarf galaxies as a new probe of dark matter interactions with ordinary matter, Phys. Rev. D **103**, 123028 (2021).

[94] D. Wadekar and Z. Wang, Constraining axion and compact dark matter with interstellar medium heating, Phys. Rev. D **107**, 083011 (2023).

[95] S. D. McDermott, H.-B. Yu, and K. M. Zurek, Turning off the lights: How dark is dark matter?, Phys. Rev. D **83**, 063509 (2011).

[96] H. Winch, J. Setford, J. Bovy, and D. Curtin, Using LSST microlensing to constrain dark compact objects in spherical and disk configurations, Astrophys. J. **933**, 177 (2022).